The molecular and cellular mechanisms associated with the destruction of terminal bronchioles in COPD

Feng Xu[1], Dragoş M. Vasilescu ![ORCID][1], Daisuke Kinose[1,2], Naoya Tanabe ![ORCID][1,3], Kevin W. Ng[4], Harvey O. Coxson[1], Joel D. Cooper[5], Tillie-Louise Hackett[1], Stijn E. Verleden[6], Bart M. Vanaudenaerde[7], Christopher S. Stevenson[8], Marc E. Lenburg[9], Avrum Spira[9], Wan C. Tan[1], Don D. Sin[1], Raymond T. Ng[1,10] and James C. Hogg[1]

[1]The Centre for Heart Lung Innovation, The University of British Columbia, located at St Paul's Hospital, Vancouver, BC, Canada. [2]Division of Respiratory Medicine, Department of Medicine, Shiga University of Medical Science, Shiga, Japan. [3]Dept of Respiratory Medicine, Graduate School of Medicine, Kyoto University, Kyoto, Japan. [4]The Francis Crick Institute, London, UK. [5]Division of Thoracic Surgery, University of Pennsylvania, Philadelphia, PA, USA. [6]Laboratory of Respiratory Diseases, BREATHE, Dept of CHROMETA, KU Leuven, Leuven, Belgium. [7]Leuven Lung Transplant Unit, KU Leuven and UZ Gasthuisberg, Leuven, Belgium. [8]Lung Cancer Initiative at Johnson and Johnson, London, UK. [9]Division of Computational Biomedicine, Dept of Medicine, Boston University, Boston, MA, USA. [10]Dept of Computer Science, The University of British Columbia, Vancouver, BC, Canada.

Corresponding author: James C. Hogg (Jim.Hogg@hli.ubc.ca)

Shareable abstract (@ERSpublications)
In COPD, terminal bronchiole destruction begins in regions of microscopic emphysema that cannot be visualised by routine thoracic CT. The over-activation of inflammatory immune responses in the diseased region might be the cause of the destruction. https://bit.ly/3l7BGNB

Abstract

Rationale Peripheral airway obstruction is a key feature of chronic obstructive pulmonary disease (COPD), but the mechanisms of airway loss are unknown. This study aims to identify the molecular and cellular mechanisms associated with peripheral airway obstruction in COPD.

Methods Ten explanted lung specimens donated by patients with very severe COPD treated by lung transplantation and five unused donor control lungs were sampled using systematic uniform random sampling (SURS), resulting in 240 samples. These samples were further examined by micro-computed tomography (CT), quantitative histology and gene expression profiling.

Results Micro-CT analysis showed that the loss of terminal bronchioles in COPD occurs in regions of microscopic emphysematous destruction with an average airspace size of $\geqslant 500$ and <1000 µm, which we have termed a "hot spot". Based on microarray gene expression profiling, the hot spot was associated with an 11-gene signature, with upregulation of pro-inflammatory genes and downregulation of inhibitory immune checkpoint genes, indicating immune response activation. Results from both quantitative histology and the bioinformatics computational tool CIBERSORT, which predicts the percentage of immune cells in tissues from transcriptomic data, showed that the hot spot regions were associated with increased infiltration of CD4 and CD8 T-cell and B-cell lymphocytes.

Interpretation The reduction in terminal bronchioles observed in lungs from patients with COPD occurs in a hot spot of microscopic emphysema, where there is upregulation of *IFNG* signalling, co-stimulatory immune checkpoint genes and genes related to the inflammasome pathway, and increased infiltration of immune cells. These could be potential targets for therapeutic interventions in COPD.

Introduction

Early studies of chronic obstructive pulmonary disease (COPD) have shown that the small conducting airways (<2 mm in diameter) only account for 10% of the total resistance to airflow in healthy adult human lungs [1]. Subsequent studies have shown that the same small airways that offer so little resistance to airflow in the normal lungs become the major site of airflow obstruction in lungs from people affected by COPD, mainly due to increased small airways resistance, increasing by up to 40-fold in severe cases [2].

Based on these and other data, MEAD [3] postulated that the smaller conducting airways constitute a "quiet zone" within the lungs where disease can accumulate without being noticed by the patient or detected by routine pulmonary function testing or thoracic imaging [3, 4]. The use of ultra-resolution micro-computed tomography (CT) has made it possible to count the small airways, which show a 40% reduction in mild and moderate COPD, and a 70–90% reduction in very severe COPD [5, 6]. Additional studies based on pre-terminal bronchioles have shown a reduction of alveolar attachments and narrowing of pre-terminal bronchioles in very severe COPD [7, 8].

Chronic inflammation in COPD is reported to increase mucus production and stimulate the tissue repair process. Both the mucus and the excess collagen deposited during scar formation have the potential to influence the lung function of patients affected by COPD [9]. Despite this cascade of new knowledge about COPD, current treatments for COPD are primarily directed at the relief of symptoms through bronchodilation rather than at the real cause of small airway obstruction and emphysematous destruction [10]. Thus, understanding the site and molecular and cellular mechanisms of COPD pathogenesis is important to identify the underlying causes and potential therapeutic targets of COPD. We postulate that specific gene profiles are associated with the destruction of terminal bronchioles in COPD. The purpose of this report is to determine the site of and identify the molecular and cellular mechanisms associated with terminal bronchiole reduction using a combination of micro-CT, quantitative histology and gene expression profiling.

Methods

Systematic uniform random sampling (SURS) was used to sample ten explanted lung specimens donated by patients with very severe COPD treated by lung transplantation and five unused donor control lungs, resulting in 240 samples [11]. The patient demographics of each of the ten COPD and five donor control lung specimens are shown in table 1.

Specimen preparation

All explanted lungs were inflated with air to a transpulmonary pressure of 30 cm H_2O and then deflated to a pressure of 10 cm H_2O. The pressure was held constant using an underwater seal while the specimen was frozen solid using liquid nitrogen vapour (-140 to $-180°C$) and stored in a $-80°C$ freezer. Each frozen lung was then cut into 2 cm thick transverse slices and SURS was applied to obtain eight paired lung samples ($2×1.6$ cm) using a sharpened steel cylinder [5, 11, 12]. One core in each pair was prepared for micro-CT while the companion core was processed for histology examination and gene expression profiling.

Micro-CT

120 of the 240 samples were examined as previously described [5, 13]. Briefly, each sample was fixed overnight in a 1% solution of glutaraldehyde in pure acetone. The fixed samples were warmed to room

TABLE 1 Cohort demographics				
Group[#]	Age (years)	Sex	Smoking (pack-years)	FEV_1 (L)
Control	42	M	15	NA
Control	65	F	NA	NA
Control	64	M	15	NA
Control	53	M	0	NA
Control	77	M	0	NA
COPD	55	M	6	NA
COPD	39	F	18	0.38
COPD	51	M	25	0.49
COPD	55	M	9	0.68
COPD	48	M	25	0.74
COPD	77	F	45	NA
COPD	59	F	40	0.56
COPD	58	F	30	0.69
COPD	55	M	80	0.95
COPD	53	F	24	0.86

FEV_1: forced expiratory volume in 1 s; COPD: chronic obstructive pulmonary disease; NA: not available. [#]: the ten explanted lungs were from patients with severe COPD who were treated by lung transplantation and the five control donor lungs, which were not suitable for lung transplantation, were released by the Gift of Life Program, Philadelphia, USA, and the Katholieke Universiteit Leuven in Belgium.

temperature, critical point dried and examined by micro-CT [13]. Three-dimensional reconstructions of micro-CT images of each core were used to identify and count the number of terminal bronchioles per mL of lung and to measure the mean linear intercept (Lm) at ten regular intervals as previously described [5, 11].

We defined regions of the lung tissue based on three cut-offs of Lm with <500 µm representing a "normal" Lm, ⩾500<1000 µm as an intermediate Lm and >1000 µm as emphysema (figure 1a, b) [14].

Quantitative histology

The 120 companion samples located adjacent to those cores examined by micro-CT were vacuum-embedded in cryomatrix and mounted in a cryostat. 10 µm thick serial frozen sections from each of the tissue cores were used for Movat's pentachrome staining to determine the general lung architecture, and immunohistochemistry to estimate the volume fractions of neutrophils (NP57, Dako-Cytomation), macrophages (CD68, Dako-Cytomation), eosinophils (Hansel's stain), CD4 T-cells (CD4, NovoCastra Laboratories), CD8 T-cells (CD8, NovoCastra Laboratories) and B-cells (CD20, Dako-Cytomation) using automated colour segmentation (ImageScope, Leica) [7]. The organisation of T-cells and B-cells was used to identify lymphoid follicles. The ratio of airways and vessels with lymphoid follicles in each core was calculated [15].

Gene expression profiling
Microarray sample processing

RNA was extracted from 20 serial cryosections taken from each of the 120 companion samples using the RNeasy Mini Kit (Qiagen). The extracted RNA was profiled on an Affymetrix GeneChip Human Gene 1.0 ST Array (ThermoFisher). Additional details as previously described [16] are shown in the supplementary material. The gene expression data have been uploaded to the Gene Expression Omnibus (GEO) database and are available under the accession number GSE151052.

Statistical analyses
Histological and micro-CT data

Linear mixed-effect models were used to determine the associations within the same tissue core between immune cells and the following pathological indices [16]: 1) micro-CT-derived Lm value; 2) ratio of airways with lymphoid follicles to total number of airways and 3) ratio of vessels with lymphoid follicles to total vessels (supplementary methods). Multi-test p-values were corrected by Benjamini–Hochberg false discovery rate (FDR). FDR<0.1 was considered significant.

Gene profile data analyses

We used a pipeline approach to identify the hot spot gene signature as shown in figure 1c. The focus was on the genes that were related to the reduction in terminal bronchioles in areas of microscopic/mild emphysema (hot spot). We used a two-pronged analysis as follows. We determined the correlation of genes to the reduction of terminal bronchioles using a Spearman rank correlation test after excluding genes with low expression levels of <2 microarray fluorescence units in more than three samples and low expression variance of <0.1 (units 0–1) across all samples [16]. In a separate analysis, a linear mixed-effect model was used to examine all 19 718 genes to identify upregulated and downregulated genes in the hot spot region (FDR<0.1, figure 1c). The resultant signature genes were associated both with terminal bronchiole reduction and the hot spot. The potential functions of these signature genes were further explored in a human protein–protein interaction immune network [17] as described in detail in the supplementary material.

Gene Set Enrichment Analysis

Gene Set Enrichment Analysis (GSEA) was used to determine which of the signature genes were differentially expressed in the hot spot *versus* non-hot spot regions (details in the supplementary methods; supplementary figure E1). Differences were assessed using a linear mixed-effect model. Based on the identification of the most enriched gene list, additional gene expression analyses on the appropriate downstream targets were conducted.

CIBERSORT

CIBERSORT was used to assess the microarray transcriptomic data to predict the relative proportion of immune cells in the lung tissue [18] and a linear mixed-effect model was used for statistical comparison.

Results
Micro-CT: hot spot for reduction in terminal bronchioles

Figure 1a shows the number of terminal bronchioles per mL of lung across the different regions of the lung stratified based on Lm. The hot spot (Lm⩾500<1000 µm) region demonstrated a significant reduction
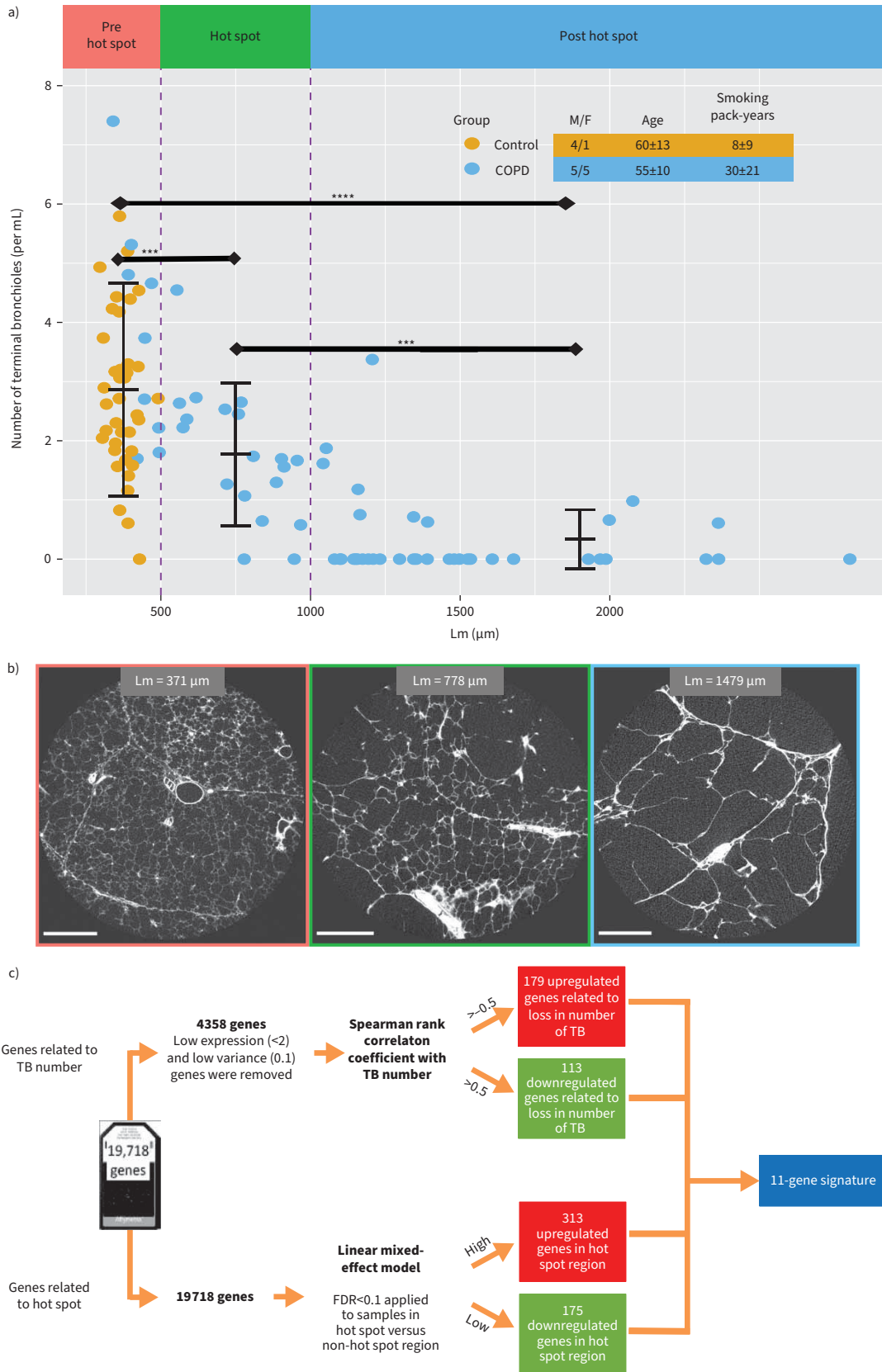
FIGURE 1 a) Identification of the hot spot region. The mean linear intercept (Lm) represents alveolar size. The two dashed vertical lines demarcate three regions of Lm: pre hot spot <500 µm; hot spot ⩾500 and <1000 µm; post hot spot ⩾1000 µm. A sharp reduction in the number of terminal bronchioles per mL of lung is detectable when Lm is ⩾500. The number of terminal bronchioles per mL of lung was significantly different between

regions as calculated using a linear-mixed-effect model. *: p<0.05; **: p<0.01; ***: p<0.005; ****: p<0.001. b) Micro-computed tomography (CT) images of a donor control sample and two chronic obstructive pulmonary disease (COPD) lung samples with Lm of 371 µm, 778 µm and 1479 µm, respectively. The colour frame around panel (b) relates to the categories in panel (a). Scale bars: 2 mm. c) Schematic flow diagram of the pipeline used to identify the 11-gene signature for the hot spot. The genes that had both strong correlations with terminal bronchiole reductions and significant differential expression in the hot spot are identified as signature genes for the hot spot in this study.

in the number of terminal bronchioles per mL of lung compared with the "pre hot spot" (Lm<500 µm) regions (p<0.005). There was an additional reduction of terminal bronchioles in the "post hot spot" (Lm⩾1000 µm) regions (p<0.001). Micro-CT analysis demonstrated that this reduction in the number of terminal bronchioles per mL of lung tissue occurred in tissue where airspace enlargement was just beyond the upper limit of normal (494 µm, figure 1a, b) [14].

Quantitative histology: immunohistochemistry

Figure 2 shows increased volume fraction of CD8 T-cells, CD4 T-cells and B-cells and decreased volume fraction of neutrophils and CD68 macrophages in the hot spot (500⩽Lm<1000 µm) and the post hot spot
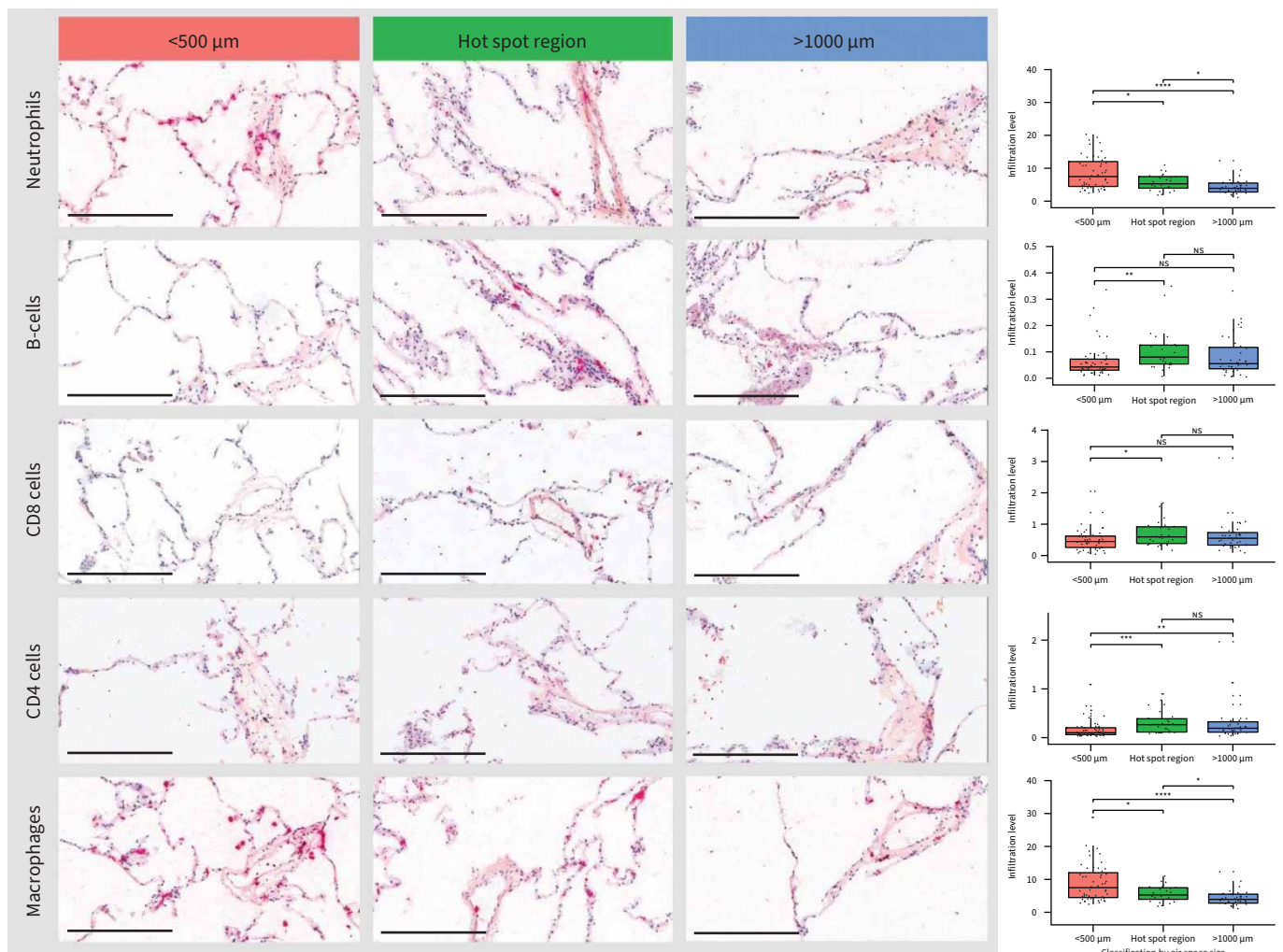

FIGURE 2 Histological data in control and chronic obstructive pulmonary disease samples. Relationship between volume fraction of immune cells (positive on immunohistochemical staining) in three regions: hot spot, pre hot spot and post hot spot demarcated by mean linear intercept (Lm). Histological slides are shown in the left panels (scale bars: 300 µm) and corresponding box plots are shown in the right panel. The volume fraction of neutrophils and macrophages decreases, while those of B-cells, CD8 T-cells and CD4 T-cells are increased in hot spot and post hot spot. Data presented as median and 5–95% quartiles. p-value calculated using a linear mixed-effect model. *: p<0.05; **: p<0.01; ***: p<0.005; ****: p<0.001.

regions compared with those in the pre hot spot (Lm<500 µm) region. The corresponding stained cells in the histological slides are also shown in figure 2.

The Lm was strongly associated with the volume fraction of CD4 T-cells and B-cells (FDR<0.1, supplementary table E1). The ratio of vessels with lymphoid follicles to total vessels was also associated with the volume fraction of CD4 and CD8 T-cells, B-cells and macrophages (FDR<0.1), whereas the ratio of airways with follicles to the total number of airways was not significantly associated with volume fraction of any of the immune cells.

Signature genes in the hot spot

Figure 1c shows the results of pipeline gene profile analysis for pre hot spot, hot spot and post hot spot regions in relation to terminal bronchioles. 113 genes were downregulated and 179 genes were upregulated with the reduction in terminal bronchioles (correlation coefficient >0.5 and <−0.5, respectively). Of all 19 718 genes, 313 were upregulated and 175 were downregulated in the hot spot (FDR<0.1, figure 1c; additional details in the supplementary material).

The 11 hot spot signature genes shown in table 2 that are also associated with terminal bronchiole reduction are those known to be involved in the tissue repair process (supplementary figure E2). Output from the human protein–protein interaction immune network showed that among these 11 genes, two genes associated with the tissue repair process were differentially regulated: *FGF10* was downregulated in the hot spot region (p<0.05) and upregulated in the post hot spot region (p<0.01), while *TGFB2* was upregulated in the hot spot (p<0.005, supplementary figure E2).

Gene Set Enrichment Analyses

GSEA identified the most significant gene list in the hot spot as the activated genes in the "HALLMARK_INTERFERON_GAMMA_RESPONSE" (supplementary figure E3) [19, 20]. In our samples, *IFNG* and its target genes, including the T-cell chemokines *CXCL9, CXCL10* and *CXCL11*, were all upregulated in the hot spot (p<0.05, figure 3a–d). *IFNGR1* was significantly downregulated in the hot spot and post hot spot regions (p<0.05, figure 3e).

Gene expression analyses on genes functionally related to the interferon-γ (IFN-γ) pathway showed there was significant upregulation of co-stimulatory immune checkpoint genes *CD40L, CD40* (p<0.001), *CD27* (p<0.001), *ICOS* (p<0.001), *CD28* and *CD80/86* (p<0.01) (figure 4a–g), but decreased expression of the co-inhibitory immune checkpoint gene *CD274* (*PDL1*, p<0.01, figure 4h) (supplementary table E2). Additionally, genes including *CASP1, NOD1* and *IL18* (involved in the inflammasome pathway) and *MAP3K14* (involved in nuclear factor-κB (NF-κB) signalling) were upregulated in the hot spot (p<0.01, supplementary figure E4a–d) [21–23], while *TREX1* was downregulated in the post hot spot (p<0.001, supplementary figure E4e).

TABLE 2 The 11 signature genes detected in the hot spot of microscopic emphysema and terminal bronchiole reduction

Gene	Fold change[#]	FDR[#]	Spearman CC with the change in TBs[¶]
FGF10	0.83	0.0365	0.50
FAM176C	0.75	0.0539	0.53
BTNL8	0.89	0.0779	0.59
AMY2B	1.03	0.0709	−0.56
GPR64	1.23	0.0130	−0.53
HCST	1.31	0.0924	−0.57
APOBEC3C	1.34	0.0072	−0.53
ISLR	1.36	0.0453	−0.53
TGFBI	1.08	0.0297	−0.53
DCSTAMP	1.57	0.0474	−0.50
GSTO1	1.04	0.0575	−0.58

FDR: false discovery rate is the expected proportion of Type 1 errors; CC: correlation coefficients; TB: terminal bronchiole. [#]: fold change (change in expression) and FDR calculated based on the comparison between the hot spot region and the non-hot spot regions; [¶]: Spearman CCs show the association between the number of terminal bronchioles and the expression level of each gene.
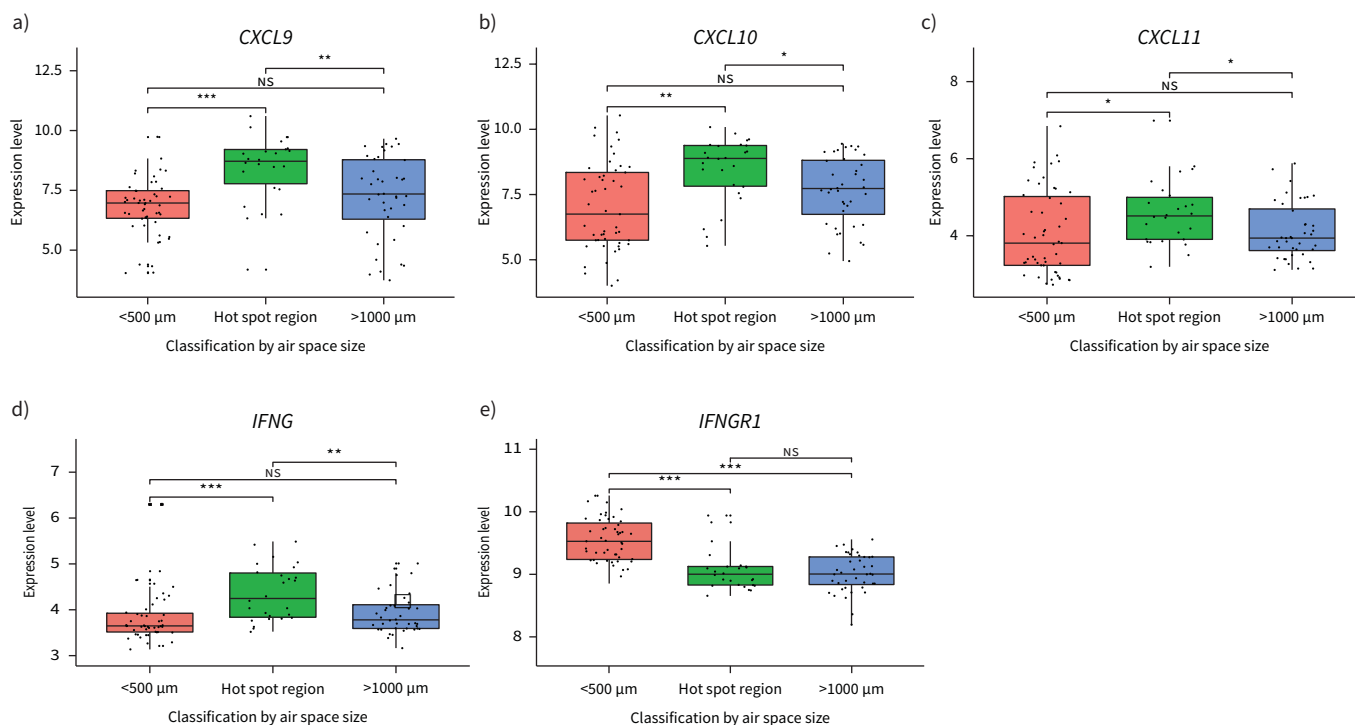
FIGURE 3 The expression patterns of interferon-γ (*IFNG*)-related genes: chemokines. a–d) *CXCL9*, *CXCL10*, *CXCL11* and *IFNG* are all upregulated in the hot spot region, while e) *IFNGR1* is downregulated in the hot spot and post hot spot region. Data presented as median and 5–95% quartiles. p-value calculated using a linear mixed-effect model. *: $p<0.05$; **: $p<0.01$; ***: $p<0.005$; ****: $p<0.001$.
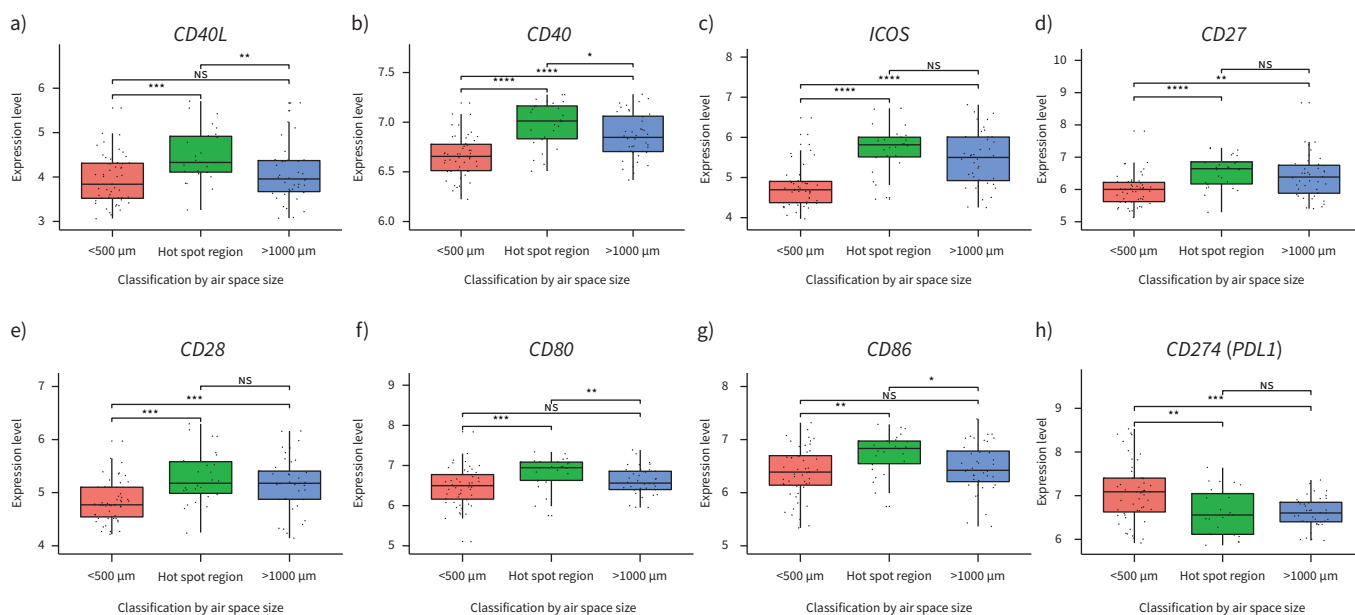

FIGURE 4 The expression patterns of interferon-γ (*IFNG*)-related genes: immune checkpoint genes. a–g) Upregulation of co-stimulatory immune checkpoint genes and h) downregulation of inhibitory immune checkpoint genes in chronic obstructive pulmonary disease samples, especially in the hot spot region. Data presented as median and 5–95% quartiles. p-value calculated using a linear mixed-effect model. *: $p<0.05$; **: $p<0.01$; ***: $p<0.005$; ****: $p<0.001$.
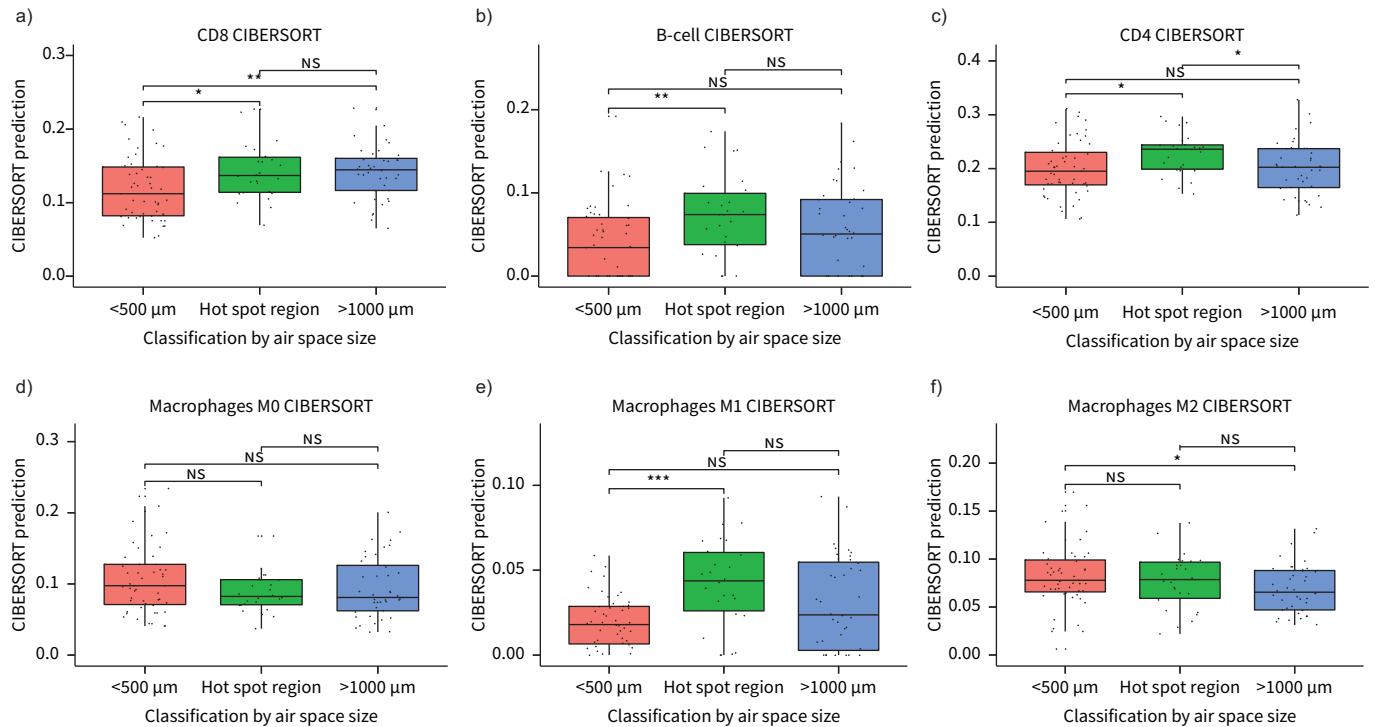
FIGURE 5 CIBERSORT prediction of increased cell subsets in control and chronic obstructive pulmonary disease samples. a–c) Increased infiltration of B-cells, CD8 T-cells and CD4 T-cells in hot spot. d–f) CIBERSORT predictions for macrophages M0 (d) and M2 (f) did not demonstrate a significant relative increase in the hot spot, while macrophage M1 (e) shows a significant increases in the hot spot region. Data presented as median and 5–95% quartiles. p-value calculated using a linear mixed-effect model. *: p<0.05; **: p<0.01; ***: p<0.005; ****: p<0.001.

CIBERSORT

CIBERSORT results confirmed those found on histology: increased infiltration of CD4 and CD8 T-cell and B-cell lymphocytes in the hot spot (p<0.05, figure 5a–c). CIBERSORT showed an increase in pro-inflammatory M1 macrophages (p<0.005) in the hot spot without significant changes in M0 and M2 macrophages (figure 5d–f).

Discussion

This study characterised the site and the molecular and cellular mechanisms associated with reduced numbers of terminal bronchioles using a combination of micro-CT, quantitative histology and gene expression profiling. To our knowledge, this is the first study focusing on small airways to use transcriptomic analyses to identify genes that are associated with specific zones of reduced terminal bronchioles within the lungs in COPD. Micro-CT data suggest that the disease begins in a hot spot that has marked reduction of terminal bronchioles in tissue with microscopic emphysema, a region beyond the detection limit of conventional CT scan. The activity in this hot spot is driven by a panel of molecular events, as indicated by a distinct gene signature, a differential gene expression profile and activation of specific immune cells validated by increased immune cell infiltration on quantitative histology. The gene signature associated with this site is consistent with that of the repetitive injury and repair process while gene expression profiling indicates that the immune system is selectively activated. The details from this study could inform research of potential targets for therapeutic interventions in COPD [24, 25].

The hot spot signature genes and their direct interactors involved in the tissue repair process support the hypothesis that the pathogenesis of COPD is driven by an aberrant tissue injury and airway remodelling process perpetuated by the inhalation of toxic particles and gases [25]. Based on the expression patterns of these genes for *FGF10* and *TGFB*, which are growth factors for the proliferation of fibroblasts, endothelial cells and specialised fibrogenic cells, we speculate that the tissue repair process involved in the remodelling of airways could lead to scar formation in airway walls [6], the contraction of which could further obliterate the airway lumen and thus explain the reduction in terminal bronchioles.

These transcriptomic analyses of tissue samples obtained using a standardised protocol of SURS of the explanted lung from patients treated by lung transplantation for COPD adds to studies based on convenience samples and surgical biopsies of lung tissue from patients with COPD [16–19]. Specifically, the gene profiles in the hot spot advance the molecular understanding of small airway disease in COPD because we identified genes upregulated in response to *IFNG* (HALLMARK_INTERFERON_GAMMA_ RESPONSE) to be the most significantly enriched gene list in the hot spot. This and the upregulation of the target chemokines *CXCL9*, *CXCL10*, *CXCL11* and the kinase *MAP3K14* concurrent with the downregulation of *IFNGR1* and *TREX1* are all consistent with previous histochemical and *in vitro* cellular studies that implicate IFN-γ stimulation and T-cell activation in COPD [15, 26–28]. The functional implications are as follows: upregulation of the chemokines, with upregulation of the kinase that could then trigger inflammation *via* the transforming growth factor-β pathway and stimulation of NF-κB activity [27]; downregulation of *IFNGR1*, affecting susceptibility to infection [29]; and downregulation of *TREX1*, which is associated with senescence-associated secretory phenotypes [30].

GSEA also yielded patterns for the regulation of immune checkpoint genes that have been documented to cause excessive T-cell inflammation in COPD [31]. Within the hot spot of microscopic emphysema and terminal bronchiolar reduction, we found evidence for activation of the adaptive immune responses in COPD, such as upregulation of co-stimulatory immune checkpoint genes, including *CD40*, and downregulation of the inhibitory immune checkpoint gene *CD274* (*PDL1*). Moreover, upregulation of the pyroptosis/inflammasome pathway-related genes, including *CASP1*, *NOD1* and *IL18*, which are critical components of the innate immune system and involved in microbial infection and cellular damage, is relevant to repeated inflammation and repair, and another potential explanation for the reduction of terminal bronchioles in patients with COPD. This activation of the immune system is further supported by increased infiltration of CD4 and CD8 T-cell and B-cell lymphocytes in the hot spot region based on quantitative histology and identification of the subset of cells by CIBERSORT in this study.

We found good agreement between the results from quantitative histology and CIBERSORT in patterns of immune cell infiltration, but CIBERSORT provided additional novel insight into differential macrophage dynamics. The quantitative histology analysis showed an overall reduction in macrophages, whereas the CIBERSORT result showed an increase of M1 but no change for M0 and M2 macrophages. Such an abnormal M1/M2 macrophage phenotype profile is associated with cytokine imbalance in the small airway wall and lumen in smokers and COPD [32] and could be an additional explanation for terminal bronchiole destruction over time.

An intriguing finding from the quantitative histology was the observation that the ratio of vessels with lymphoid follicles to total vessels is associated with the infiltration of CD8 T-cells, B-cells and macrophages (FDR<0.1), whereas the ratio of airways with follicles to the total number of airways is not similarly associated. It is conceivable that lymphoid follicles on vessels could be more easily formed than lymphoid follicles on airways. The presence of lymphoid follicles with germinal centres is indicative of an adaptive immune response, is part of the remodelling process and results in scar formation, contraction and distortion of the airways with a resulting impact on lung function in patients with COPD [33]. We speculate that preventing lymphoid follicle formation or immune cell infiltration could be an effective way of reversing the pathogenesis of COPD.

This study has several limitations. First, we were only able to examine the lungs of patients with end-stage COPD. Because it is not possible to obtain whole lungs from patients at different stages of COPD severity, we instead compared the differences in disease severity in different regions of the same lung. Second, quantitative histology could not discriminate different subtypes of macrophages and we could only rely on CIBERSORT to infer the differences among distinct macrophage phenotypes [32]. Third, the cellular components of the lung tissues in this project might be different from the samples used in a previous publication [18]. It is possible that CIBERSORT may not accurately estimate the absolute numbers of individual cells, but in this study we have focused on the relative proportions rather than absolute numbers of different immune cells in lung tissues. These findings were largely validated by immunohistochemistry [18]. Fourth, microarrays were used in this study to identify signature genes. Although microarray data correlate well with RNA-sequencing data [34, 35], it is possible that some genes, especially those that have low expression, may have been missed [36]. Despite this limitation, we believe that the data from our analyses reflect the pathological and immunological events occurring in COPD for two reasons: previous authors had shown comparable results between microarray and RNA-sequencing [34, 35, 37]; and the microarray data used in our computational models of GSEA and CIBERSORT were able to identify 1) significant differences between cases and controls, with validation by quantitative histology, and 2) key gene pathways relevant in COPD. Fifth, the number of subjects analysed in this study was relatively small owing to the study design, which

required excised lung specimens. We acknowledge that a bigger validation dataset would be needed to test for causal relationships between immune response activation, obliteration of lumen due to tissue repair and pathogenesis of COPD. Finally, the clinical relevance of immune modulation may not be as intuitive in COPD as in asthma. Yet, the use of broad-spectrum anti-inflammatories such as inhaled corticosteroids and macrolides have had modest but significant salutary effects in COPD, including reducing symptoms and the risk of exacerbations and possibly mortality [38]. However, to date, there is no conclusive clinical trial evidence that any treatment for COPD can modify the long-term decline in lung function. Our observations of immune balance in small airway pathology could be a guide for further research into new immunomodulatory treatments for COPD.

In conclusion, this study shows that terminal bronchioles are destroyed within regions of microscopic emphysema in COPD. Importantly, our data identify a gene signature that is associated with the repetitive injury and repair process. The expression patterns of genes support the concept that immune response activation in COPD might initiate tissue destruction. Activation of the immune response is further supported by the increased infiltration of immune cells in lung tissue based on both quantitative histology and CIBERSORT. These specific genes and related cellular events could be potential targets for therapeutic interventions in COPD.

References

1 Macklem PT, Mead J. Resistance of central and peripheral airways measured by a retrograde catheter. *J Appl Physiol* 1967; 22: 395–401.

2 Hogg JC, Macklem PT, Thurlbeck WM. Site and nature of airway obstruction in chronic obstructive lung disease. *N Engl J Med* 1968; 278: 1355–1360.

3 Mead J. The lung's "quiet zone". *N Engl J Med* 1970; 282: 1318–1319.

4 Hogg J, Williams J, Richardson J, *et al.* Age as a factor in the distribution of lower-airway conductance and in the pathologic anatomy of obstructive lung disease. *N Engl J Med* 1970; 282: 1283–1287.

5 McDonough JE, Yuan R, Suzuki M, *et al.* Small-airway obstruction and emphysema in chronic obstructive pulmonary disease. *N Engl J Med* 2011; 365: 1567–1575.

6 Koo H-K, Vasilescu DM, Booth S, *et al.* Small airways disease in mild and moderate chronic obstructive pulmonary disease: a cross-sectional study. *Lancet Respir Med* 2018; 6: 591–602.

7   Tanabe N, Vasilescu DM, McDonough JE, *et al.* Micro-computed tomography comparison of preterminal bronchioles in centrilobular and panlobular emphysema. *Am J Respir Crit Care Med* 2017; 195: 630–638.

8   Saetta M, Ghezzo H, Kim WD, *et al.* Loss of alveolar attachments in smokers. A morphometric correlate of lung function impairment. *Am Rev Respir Dis* 1985; 132: 894–900.

9   Hogg JC, Pare PD, Hackett TL. The contribution of small airway obstruction to the pathogenesis of chronic obstructive pulmonary disease. *Physiol Rev* 2017; 97: 529–552.

10 Vogelmeier CF, Criner GJ, Martinez FJ, *et al.* Global strategy for the diagnosis, management, and prevention of chronic obstructive lung disease 2017 report. GOLD executive summary. *Am J Respir Crit Care Med* 2017; 195: 557–582.

11 Vasilescu DM, Phillion AB, Kinose D, *et al.* Comprehensive stereological assessment of the human lung using multi-resolution computed tomography. *J Appl Physiol (1985)* 2020; 128: 1604–1616.

12 Verleden SE, Vasilescu DM, Willems S, *et al.* The site and nature of airway obstruction after lung transplantation. *Am J Respir Crit Care Med* 2014; 189: 292–300.

13 Vasilescu DM, Phillion AB, Tanabe N, *et al.* Nondestructive cryomicro-CT imaging enables structural and molecular analysis of human lung tissue. *J Appl Physiol (1985)* 2017; 122: 161–169.

14 Xu F, Vasilescu DM, Kinose D, *et al.* A morphometric "hot spot" for terminal bronchiolar destruction in COPD. *Am J Respir Crit Care Med* 2018; 197: A7364.

15 Hogg JC, Chu F, Utokaparch S, *et al.* The nature of small-airway obstruction in chronic obstructive pulmonary disease. *N Engl J Med* 2004; 350: 2645–2653.

16 Campbell JD, McDonough JE, Zeskind JE, *et al.* A gene expression signature of emphysema-related lung destruction and its reversal by the tripeptide GHK. *Genome Med* 2012; 4: 67.

17 Faner R, Cruz T, Casserras T, *et al.* Network analysis of lung transcriptomics reveals a distinct B-cell signature in emphysema. *Am J Respir Crit Care Med* 2016; 193: 1242–1253.

18 Newman AM, Liu CL, Green MR, *et al.* Robust enumeration of cell subsets from tissue expression profiles. *Nat Methods* 2015; 12: 453–457.

19 Subramanian A, Tamayo P, Mootha VK, *et al.* Gene set enrichment analysis: a knowledge-based approach for interpreting genome-wide expression profiles. *Proc Natl Acad Sci USA* 2005; 102: 15545–15550.

20 Liberzon A, Birger C, Thorvaldsdottir H, *et al.* The Molecular Signatures Database (MSigDB) hallmark gene set collection. *Cell Syst* 2015; 1: 417–425.

21 Miao EA, Rajan JV, Aderem A. Caspase-1-induced pyroptotic cell death. *Immunol Rev* 2011; 243: 206–214.

22 Suzuki T, Franchi L, Toma C, *et al.* Differential regulation of caspase-1 activation, pyroptosis, and autophagy via Ipaf and ASC in Shigella-infected macrophages. *PLoS Pathog* 2007; 3: e111.

23 Davis BK, Wen H, Ting JP. The inflammasome NLRs in immunity, inflammation, and associated diseases. *Annu Rev Immunol* 2011; 29: 707–735.

24 Vinay Kumar AKA, Nelson F, Robbins SL, *et al.* Robbins and Cotran Pathologic Basis of Disease. 7th Edn. Philadelphia, Elsevier Saunders, 2004.

25 Hogg JC, McDonough JE, Gosselink JV, *et al.* What drives the peripheral lung-remodeling process in chronic obstructive pulmonary disease? *Proc Am Thorac Soc* 2009; 6: 668–672.

26 Kim WD, Chi HS, Choe KH, *et al.* A possible role for CD8^{+} and non-CD8^{+} cell granzyme B in early small airway wall remodelling in centrilobular emphysema. *Respirology* 2013; 18: 688–696.

27 Levi-Schaffer F, Garbuzenko E, Rubin A, *et al.* Human eosinophils regulate human lung- and skin-derived fibroblast properties *in vitro*: a role for transforming growth factor-β (TGF-β). *Proc Natl Acad Sci USA* 1999; 96: 9660–9665.

28 Barnes PJ. Immunology of asthma and chronic obstructive pulmonary disease. *Nat Rev Immunol* 2008; 8: 183–192.

29 Skrenta H, Yang Y, Pestka S, *et al.* Ligand-independent down-regulation of IFN-λ receptor 1 following TCR engagement. *J Immunol* 2000; 164: 3506–3511.

30 De Cecco M, Ito T, Petrashen AP, *et al.* Author correction: L1 drives IFN in senescent cells and promotes age-associated inflammation. *Nature* 2019; 572: E5.

31 Wilkinson TMA. Immune checkpoints in chronic obstructive pulmonary disease. *Eur Respir Rev* 2017; 26: 170045.

32 Eapen MS, Hansbro PM, McAlinden K, *et al.* Abnormal M1/M2 macrophage phenotype profiles in the small airway wall and lumen in smokers and chronic obstructive pulmonary disease (COPD). *Sci Rep* 2017; 7: 13392.

33 Siafakas NM, Antoniou KM, Tzortzaki EG. Role of angiogenesis and vascular remodeling in chronic obstructive pulmonary disease. *Int J Chron Obstruct Pulmon Dis* 2007; 2: 453–462.

34 Rao MS, Van Vleet TR, Ciurlionis R, *et al.* Comparison of RNA-seq and microarray gene expression platforms for the toxicogenomic evaluation of liver from short-term rat toxicity studies. *Front Genet* 2018; 9: 636.

35 Ditz B, Boekhoudt JG, Aliee H, *et al.* Comparison of genome-wide gene expression profiling by RNA sequencing versus microarray in bronchial biopsies of COPD patients before and after inhaled corticosteroid treatment: does it provide new insights? *ERJ Open Res* 2021; 7: 00104-2021.

36   Li J, Hou R, Niu X, *et al.* Comparison of microarray and RNA-seq analysis of mRNA expression in dermal mesenchymal stem cells. *Biotechnol Lett* 2016; 38: 33–41.

37   Wang C, Gong B, Bushel PR, *et al.* The concordance between RNA-seq and microarray data depends on chemical treatment and transcript abundance. *Nat Biotechnol* 2014; 32: 926–932.

38   Halpin DMG, Criner GJ, Papi A, *et al.* Global initiative for the diagnosis, management, and prevention of chronic obstructive lung disease. The 2020 GOLD Science Committee report on COVID-19 and chronic obstructive pulmonary disease. *Am J Respir Crit Care Med* 2021; 203: 24–36.